



# Relative stability of the $S_2$ isomers of the oxygen evolving complex of photosystem II

Divya Kaur<sup>1,2</sup> · Witold Szejgis<sup>2</sup> · Junjun Mao<sup>2</sup> · Muhamed Amin<sup>3</sup> · Krystle M. Reiss<sup>4</sup> · Mikhail Askerka<sup>4</sup> · Xiuhong Cai<sup>2,5</sup> · Umesh Khaniya<sup>2,5</sup> · Yingying Zhang<sup>2,5</sup> · Gary W. Brudvig<sup>4</sup> · Victor S. Batista<sup>4</sup> · M. R. Gunner<sup>1,2,5</sup>

Received: 7 December 2018 / Accepted: 15 March 2019 / Published online: 2 April 2019  
© Springer Nature B.V. 2019

## Abstract

The oxidation of water to  $O_2$  is catalyzed by the Oxygen Evolving Complex (OEC), a  $Mn_4CaO_5$  complex in Photosystem II (PSII). The OEC is sequentially oxidized from state  $S_0$  to  $S_4$ . The  $S_2$  state,  $(Mn^{III})(Mn^{IV})_3$ , coexists in two redox isomers:  $S_{2,g=2}$ , where Mn4 is  $Mn^{IV}$  and  $S_{2,g=4,1}$ , where Mn1 is  $Mn^{IV}$ . Mn4 has two terminal water ligands, whose proton affinity is affected by the Mn oxidation state. The relative energy of the two  $S_2$  redox isomers and the protonation state of the terminal water ligands are analyzed using classical multi-conformer continuum electrostatics (MCCE). The Monte Carlo simulations are done on QM/MM optimized  $S_1$  and  $S_2$  structures docked back into the complete PSII, keeping the protonation state of the protein at equilibrium with the OEC redox and protonation states. Wild-type PSII, chloride-depleted PSII, PSII in the presence of oxidized  $Y_Z$ /protonated D1-H190, and the PSII mutants D2-K317A, D1-D61A, and D1-S169A are studied at pH 6. The wild-type PSII at pH 8 is also described. In qualitative agreement with experiment, in wild-type PSII, the  $S_{2,g=2}$  redox isomer is the lower energy state; while chloride depletion or pH 8 stabilizes the  $S_{2,g=4,1}$  state and the mutants D2-K317A, D1-D61A, and D1-S169A favor the  $S_{2,g=2}$  state. The protonation states of D1-E329, D1-E65, D1-H337, D1-D61, and the terminal waters on Mn4 (W1 and W2) are affected by the OEC oxidation state. The terminal W2 on Mn4 is a mixture of water and hydroxyl in the  $S_{2,g=2}$  state, indicating the two water protonation states have similar energy, while it remains neutral in the  $S_1$  and  $S_{2,g=4,1}$  states. In wild-type PSII, advancement to  $S_2$  leads to negligible proton loss and so there is an accumulation of positive charge. In the analyzed mutations and  $Cl^-$  depleted PSII, additional deprotonation is found upon formation of  $S_2$  state.

**Keywords** Grand canonical Monte Carlo simulations · Linear response approximation (LRA) · Oxygen evolving complex (OEC) ·  $pK_a$  · Photosystem II · Proton transfer

**Electronic supplementary material** The online version of this article (<https://doi.org/10.1007/s11120-019-00637-6>) contains supplementary material, which is available to authorized users.

✉ M. R. Gunner  
mgunner@ccny.cuny.edu

<sup>1</sup> Department of Chemistry, The Graduate Center of the City University of New York, New York, NY 10016, USA

<sup>2</sup> Department of Physics, City College of New York, 160 Convent Avenue, New York, NY 10031, USA

<sup>3</sup> University of Groningen, Nijenborgh 4, 9747 AG Groningen, The Netherlands

<sup>4</sup> Department of Chemistry, Yale University, New Haven, CT 06520, USA

<sup>5</sup> Department of Physics, The Graduate Center of the City University of New York, New York, NY 10016, USA

## Introduction

Oxygenic photosynthesis stores solar energy as reduced products used to fix carbon as well as in the form of a trans-membrane electrochemical potential gradient that enables synthesis of ATP. Photosystem II (PSII) contains the oxygen evolving complex (OEC) a remarkable catalyst composed of earth abundant Mn and Ca that oxidizes water at room temperature and physiological pH (Dau et al. 2012; Renger 2012; Cox et al. 2013; Cox and Messinger 2013). Thus, PSII uses water, the universal biological solvent, as the ultimate metabolic electron source (Yano and Yachandra 2014; Debus 2015; Vinyard and Brudvig 2017). The resultant  $O_2$  is a by-product that sustains aerobic life on Earth. The reaction cycle accumulates four oxidizing equivalents in the OEC before evolving  $O_2$  in a single redox step, with

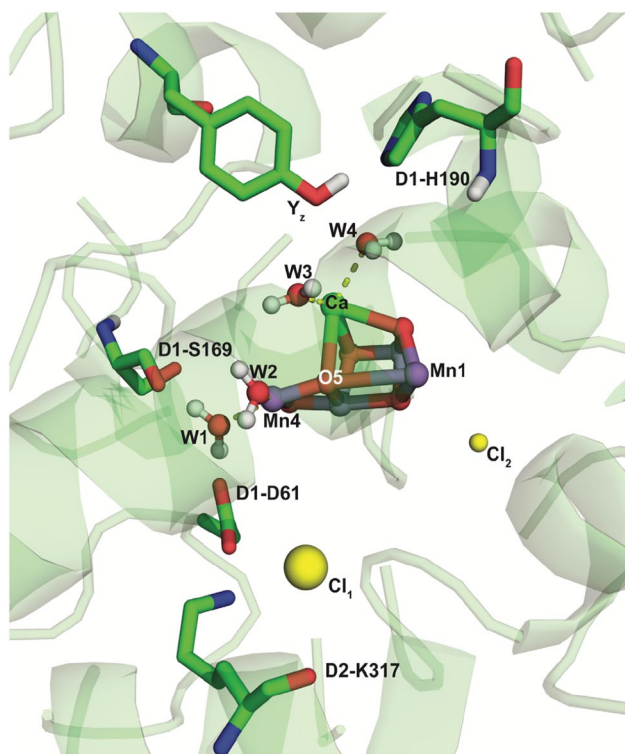


**Fig. 1** Key residues around the  $\text{Mn}_4\text{CaO}_5$  OEC, including D2-K317, D1-D61, D1-S169, D1-H190, and  $\text{Y}_z$ ;  $\text{Cl}_1$ ,  $\text{Cl}_2$  are represented as spheres. Terminal water ligands of Mn4 (W1 and W2) and  $\text{Ca}^{\text{II}}$  (W3 and W4) are explicitly shown. Mn1 and Mn4 are shown on the front face of the OEC with Mn4 on the left, Mn1 on the right, and O5 in between them. The OEC is in the optimized  $\text{S}_1(3443)$  configuration as obtained by DFT-QM/MM calculations (Luber et al. 2011), determined within a 15 Å sphere of residues from the D1, D2, and CP43 subunits derived from the 3ARC structure (Umena et al. 2011)

explicit changes of the cluster structure coupled to cluster deprotonation and water addition. Combining computational analysis with new atomic structures of the OEC (Suga et al. 2015; Kern et al. 2018) is providing an emerging picture of the mechanism.

The OEC is a  $\text{Mn}_4\text{CaO}_5$  cluster in a cubane-like structure with three high-valent Mn centers and  $\text{Ca}^{\text{II}}$  connected to a fourth, dangler manganese through  $\mu$ -oxo bridges (Fig. 1) (Umena et al. 2011; Kern et al. 2018). Four terminal waters are bound to the OEC, two coordinated to Mn4 (W1, W2) and two to  $\text{Ca}^{\text{II}}$  (W3, W4). Upon loss of four electrons, the OEC oxidizes two waters to  $\text{O}_2$  in one step, without generating high energy, intermediate reactive oxygen species (Kok et al. 1970). The OEC thus cycles through five S-states,  $\text{S}_0$ – $\text{S}_4$ , with  $\text{S}_0$  and  $\text{S}_4$  the most reduced and most oxidized intermediates, respectively.  $\text{S}_1$ , with one less electron than  $\text{S}_0$ , is the stable dark-adapted state (Joliot 2005). Four protons are lost through the Kok cycle of S-state transitions as the OEC is oxidized (Dau and Haumann 2007; Dau et al. 2012). In the overall reaction, the protons are lost from the

substrate water (Siegbahn 2013a). However, during each S-state transition, protons can be lost from bridging oxygens or terminal water ligands within the OEC or from surrounding residues in the protein. Proton loss can make oxidation more favorable, since it diminishes the buildup of positive charge. One proton is released on the oxidation of  $\text{S}_0$  and  $\text{S}_2$  (Rappaport and Lavergne 1991; Lavergne and Junge 1993; Suzuki et al. 2009; Dau et al. 2012), but the oxidation of  $\text{S}_1$  to  $\text{S}_2$  releases significantly less than one proton to the outside of the protein. It is unknown if there is internal protein rearrangement on this step.

The  $\text{S}_1$  intermediate is the most stable state in the dark (Luber et al. 2011; Davis and Pushkar 2015; Kern et al. 2018),  $\text{S}_2$  has two redox isomers with distinctive EPR signals (Dismukes and Siderer 1981; Casey and Sauer 1984; Zimmermann and Rutherford 1984; De Paula and Brudvig 1985). If the bridging oxygen (O5) completes the coordination shell of Mn4, then the OEC redox isomer with only Mn1 remaining  $\text{Mn}^{\text{III}}$  ( $\text{Mn1}^{\text{III}}\text{Mn2}^{\text{IV}}\text{Mn3}^{\text{IV}}\text{Mn4}^{\text{IV}}$  denoted 3444) is formed which shows the characteristic EPR multiline spectra at  $g=2$  (denoted  $\text{S}_{2,g=2}$ ). However, when O5 moves closer to Mn1 closing the cube, then Mn1 is oxidized and the 4443 redox isomer is formed, which has a broad EPR signal at  $g=4.1$  ( $\text{S}_{2,g=4.1}$ ) (Pantazis et al. 2012; Bovi et al. 2013; Narzi et al. 2014; Krewald et al. 2015). The relative stability of these two isomers is influenced by the surrounding environment (Pokhrel and Brudvig 2014). For example, higher pH (Boussac et al. 2018) or chloride depletion favors the  $\text{S}_{2,g=4.1}$  isomer (Ono et al. 1986; Amin et al. 2016), while the D2-K317A (Pokhrel et al. 2013), D1-D61A (Debus 2014), and D1-S169A (Askerka et al. 2015a) mutations stabilize the  $\text{S}_{2,g=2}$  isomer. In the  $\text{S}_2$  to  $\text{S}_3$  transition, the addition of a substrate water to either Mn1 (Siegbahn 2013a; Cox and Messinger 2013) or Mn4 (Askerka et al. 2015a; Wang et al. 2017) is thought to complete the OEC ligation.

We apply the Multi-Conformer Continuum Electrostatics (MCCE) methodology (Song et al. 2009) optimized for the study of Mn complexes (Amin et al. 2013) to explore the protonation state changes of residues around the OEC. While MCCE uses a simple, classical electrostatics description, it allows sampling of side chain and water positions as well as protonation and oxidation states keeping the protein and OEC in equilibrium. We use the Linear Response Approximation (LRA) (Makri 1999) to find the relative midpoint potential ( $E_m$ ) of the two  $\text{S}_2$  redox isomers. The simulations show that all four terminal water ligands are fully protonated in  $\text{S}_1$ , while W2 is partially deprotonated in  $\text{S}_{2,g=2}$  with  $\text{Mn4}^{\text{IV}}$ , but remains protonated in  $\text{S}_{2,g=4.1}$  with  $\text{Mn4}^{\text{III}}$ . The small overall proton loss (Suzuki et al. 2009) during the  $\text{S}_1$  to  $\text{S}_2$  transition is identified as being due to D1-E329 and D1-D61 binding much of the proton released from W2 in the ensemble of states obtained by Monte Carlo sampling. We analyze how deprotonation is affected by oxidation of

$Y_Z$  with concomitant proton transfer to D1-H190, raising the pH from 6 to 8, depletion of chloride, and the site-directed mutations D2-K317A, D1-D61A, and D1-S169A. The calculated trends for how these perturbations modify the free energy difference between the two  $S_2$  redox isomers are found to be consistent with experiments.

## Methods

Calculations start with coordinates extracted from 3ARC (Umena et al. 2011), the 1.9 Å X-ray crystal structure of *Thermosynechococcus vulcanus* PSII. The QM/MM sphere used for optimization consists of the OEC and a sphere with a diameter of  $\approx 15$  Å consisting of residues centered at the OEC from the D1, D2, and CP43 subunits (Luber et al. 2011; Askerka et al. 2014, 2015a, b, 2016). The residues in the sphere are as follows: D1 (chain A): (57)-V58-V67-(68), (81)-V82-L91-(92), (107)-N108-Y112-(113), (155)-A156-I192-(193), (289)-I290-N298-(299), (323)-A324-A344:C-terminus; CP43 (chain C): (290)-W291-(292), (305)-G306-A314-(315), (334)-T335-L337-(338), (341)-M342-(343), (350)-F351-F358-(359), (398)-A399-G402-(403), (408)-G409-E413-(414); D2 (chain D): (311)-E312-L321-(322), (347)-R348-L352:C-terminus. For the capping residues, in parenthesis, only the backbone atoms are considered. The two crystallographic chloride ions are included:  $Cl_1$  near D2-K317, and  $Cl_2$  near N338 and F339 (Fig. 1).

The DFT-QM/MM methodology was used to optimize the OEC in the  $S_1$  (Mn oxidation 3443) (Luber et al. 2011),  $S_{2,g=2}$  (3444), and  $S_{2,g=4.1}$  (4443) states (Askerka et al. 2014). The nomenclature will use a subscript to describe the MCCE oxidation state of each Mn and a superscript to describe the S-state in which the structure was optimized within QM/MM.<sup>1</sup> The RMSD when comparing the  $Mn_4CaO_5$  atoms for the  $S^1$  and two  $S^2$  structures as well as surrounding protein is very small. Each QM/MM optimized structure was then docked back into the 3ARC (Umena et al. 2011) PSII protein for classical electrostatic MCCE calculations.

MCCE (Song et al. 2009) and similar programs (Ullmann and Knapp 1999; Baker et al. 2001; Wang et al. 2015) use continuum electrostatics energies and Monte Carlo sampling to estimate the protonation equilibria proteins (Gunner et al.

2011; Nielsen et al. 2011). MCCE has been tested for the analysis of  $pK_a$ s (Song et al. 2009; Gunner et al. 2011), of Mn model complexes (Amin et al. 2013), the OEC in PSII (Amin et al. 2015), as well as for anion binding (Song and Gunner 2009; Chenal and Gunner 2017). The MCCE calculations keep the protein in equilibrium with the OEC in each state. MCCE has its own limitations. MCCE considers only electrostatic and van der Waals interactions and does not include any quantum mechanical effects, such as the important Jahn–Teller distortions in the coordination sphere of  $Mn^{III}$  centers that need to be informed by DFT-QM/MM calculations. In addition, the protein backbone and the OEC coordinates are kept fixed during MCCE Monte Carlo sampling. The MCCE isosteric sampling (Song et al. 2009) is applied as described previously for PSII (Amin et al. 2015). C, O, and N side chain positions are fixed, allowing sampling of ionized and neutral protonation states of Asp, Glu, Arg, Lys, His, and Tyr. Alternative positions for hydroxyl protons, exchanged Asn and Gln terminal O and N, and His tautomers are sampled. Crystallographic waters are removed from the protein and modeled by implicit solvent. The 166 explicit waters (including the four water ligands to  $Mn_4$  and  $Ca^{II}$ ) within the 15 Å sphere surrounding the OEC that were included in the QM/MM optimization are retained. In QM/MM, each water has a single set of proton positions, while in MCCE each input water oxygen samples at least 20 possible proton positions (including those found in the QM/MM structure) as well as a conformer where it has been moved out of the protein into the bulk solvent. The waters ligated to the  $Mn_4$  (W1, W2) or  $Ca^{II}$  (W3, W4) can be  $H_2O$  or  $OH^-$  with rotating proton positions but must remain bound. The ligands directly attached to the OEC, including D1-E189, D1-E333, D1-D342, and CP43-E354 are deprotonated while D1-H332 is neutral in our calculations (Luber et al. 2011).

Parse charges, optimized for continuum electrostatic calculations (Tannor et al. 1994), are used for amino acids, including the amino acid ligands, while valence charges are used for the OEC (Amin et al. 2015). Cofactors such as chlorophyll, pheophytin, heme, non-heme iron, and  $Cl^-$  use standard MCCE topology files (Amin et al. 2015). All cofactors other than the OEC are kept in their neutral state. TIPS (Jorgensen 1981) charges are used for explicit water. Delphi Poisson–Boltzmann electrostatic energies are calculated, with a dielectric constant  $\epsilon = 4$  for the protein, and  $\epsilon = 80$  for implicit solvent water. Amber van der Waals parameters are used, reduced to 25% of their full value as suggested in previous MCCE benchmark calculations (Gunner et al. 2011). Cavities with a radius  $\geq 1.4$  Å are filled with a dielectric constant  $\epsilon = 80$ . The implicit salt concentration is 0.15 M with a 2 Å Stern layer. The default pH = 6. The Boltzmann distribution for all degrees of freedom is obtained by Grand Canonical Monte Carlo (GCMC) sampling.

<sup>1</sup> The subscript refers to the redox state ( $S_1$ ,  $S_{2,g=2}$ ,  $S_{2,g=4.1}$ ) while the superscript refers to the input S-state structure in which the OEC is optimized by QM/MM ( $S^1$ ,  $S^{2,g=2}$  and  $S^{2,g=4.1}$ ). For example,  $S_1^{2,g=2}$  identifies the QM/MM  $S^{2,g=2}$  structure (with its geometry optimized in the open cubane 3444 state as the input structure for the MCCE classical analysis of the cluster in the 3443  $S_1$  redox state. The four numbers denote the redox state of each Mn. Thus, 3443 indicates the OEC state  $Mn^{III}Mn^{IV}Mn^{IV}Mn^{IV}$ .

The relative energies of the  $S_1$  and  $S_2$  isomers are determined by MCCE calculations as a function of pH and  $E_h$  (Mao et al. 2003; Zhu and Gunner 2005; Amin et al. 2013). The free energy difference obtained from MCCE calculations is compared to the DFT-QM/MM free energy (Becke 1988) as described in SI Section VII. For chloride-depleted calculations, both chloride ions are forced into solution during Monte Carlo sampling (Song and Gunner 2009; Chenal and Gunner 2017). Site-directed mutations, D2-K317A, D1-D61A, and D1-S169A, are carried out within MCCE where these side chains are mutated to alanine using the residue completion subroutine, keeping the protein backbone fixed. Cavities formed by mutations are also filled with implicit water (Song et al. 2009). For D2-K317A, different  $Cl^-$  positions were generated using the translation subroutine of MCCE to determine if chloride is repositioned by the mutation (Fig. S3) (Song and Gunner 2009). The binding affinity of  $Cl_1$ , near the OEC, is calculated in the  $S^1$  structure at pH 6 by varying the  $Cl^-$  chemical potential (Song and Gunner 2009; Chenal and Gunner 2017). The comparison of calculations in full PSII protein and QM/MM sphere at pH 6 is reported in Table S2.

## Results

MCCE Monte Carlo sampling generates a Boltzmann distribution of redox states for the four Mn centers of the OEC in their III or IV oxidation states, corresponding to the  $S_1$ ,  $S_{2,g=2}$ , and  $S_{2,g=4.1}$  intermediates in their DFT-QM/MM optimized  $S^1$ ,  $S_{2,g=2}^{2,g=2}$ , and  $S_{2,g=4.1}^{2,g=4.1}$  configurations (Luber et al. 2011; Askerka et al. 2014) (see footnote 1 for a description of the nomenclature). There are twelve possible  $S_1$  ( $(Mn^{III})_2(Mn^{IV})_2$ ) states representing the distinguishable assignments for two  $Mn^{III}$  and two  $Mn^{IV}$  over the four Mn sites. The  $S_1$  state found by Monte Carlo sampling is 3443, independent of the input structure. Thus, less than 0.1% of the accepted microstates have a different redox assignment for the individual Mn, indicating that the alternative states are at least 180 meV higher in energy. There are four possible  $S_2$  ( $(Mn^{III})_1(Mn^{IV})_3$ ) states and starting with the  $S^1$  or  $S_{2,g=2}^{2,g=2}$  structures only the 3444,  $S_{2,g=2}^{2,g=2}$  redox isomer is found (Table 1). Starting with the  $S_{2,g=4.1}^{2,g=4.1}$  structure, the cluster adopts the expected 4443,  $S_{2,g=4.1}^{2,g=4.1}$  redox isomer. In the  $S_{2,g=2}^{2,g=2}$  input structure, the bridging  $O5^{2-}$  is closer to Mn4, while it is closer to Mn1 in the  $S_{2,g=4.1}^{2,g=4.1}$  structure. In MCCE, the electrostatic interaction with  $O5^{2-}$  helps in determining whether Mn1 or Mn4 will be oxidized. The  $S_1$  or  $S_2$  redox isomer selected by Monte Carlo sampling is independent of the protonation state of waters ligated to Mn4 and  $Ca^{II}$ .

**Table 1** Lowest energy redox isomers for  $S_1$  and  $S_2$  in each QM/MM optimized structure

| Structure               | $(Mn^{III})_2(Mn^{IV})_2$ | $Mn^{III}(Mn^{IV})_3$ |
|-------------------------|---------------------------|-----------------------|
|                         | $S_1$                     | $S_2$                 |
| $S^1$                   | 3443                      | 3444                  |
| $S_{2,g=2}^{2,g=2}$     | 3443                      | 3444                  |
| $S_{2,g=4.1}^{2,g=4.1}$ | 3443                      | 4443                  |
| Isomers <sup>a</sup>    | 12                        | 4                     |

Lowest energy oxidation states III or IV for Mn1, Mn2, Mn3, Mn4. The expected redox isomer is in italicis (Dismukes and Siderer 1981; De Paula and Brudvig 1985; Krewald et al. 2015)

<sup>a</sup>Isomers: number of possible ways to assign the oxidation states to the four Mn to create  $S_1$  ( $(Mn^{III})_2(Mn^{IV})_2$ ) or  $S_2$  ( $(Mn^{III})(Mn^{IV})_3$ )

### Protonation states of water ligands of Mn4 in $S_1$ , $S_{2,g=2}^{2,g=2}$ and $S_{2,g=4.1}^{2,g=4.1}$

The protonation states of all residues and terminal water ligands optimized in the  $S^1$  and two  $S^2$  structures were docked into the full PSII. Table 2 reports the residues that are within  $\approx 8 \text{ \AA}$  of the OEC (the residues in the region for QM/MM optimization) that change in  $S_1^1$ ,  $S_{2,g=2}^{2,g=2}$ , and  $S_{2,g=4.1}^{2,g=4.1}$  states. Other residues within this region whose protonation state do not change in any S-state, or with any perturbation including raising the pH to 8, are D1-D59, R64, R334, E308, E312, R348, which remain ionized, while D1-Y112, Y<sub>2</sub>161, H190, E413, Y315 remain neutral. The changes in protonation probabilities are relatively independent of the input structure (Table S1).

The Boltzmann distribution of protonation states of terminal waters are observed in each S-state. While W3 and W4 bound to  $Ca^{II}$  have the freedom to lose a proton, they remain neutral. W1 and W2 ligated to Mn4 are neutral in  $S_1$ , independent of which input structure is used. In the  $S_{2,g=2}^{2,g=2}$  redox state, Mn4 is oxidized to  $Mn^{IV}$ , which lowers the  $pK_a$  of W2, leading to a significant fraction of microstates having W2 as a hydroxyl. Calculations indicate that the probability of water deprotonation is  $80\% \pm 0.03$  in  $S_{2,g=2}^{2,g=2}$  while it is  $94\% \pm 0.10$  when the calculations use the  $S^1$  or  $S_{2,g=4.1}^{2,g=4.1}$  structures with the 3444,  $S_{2,g=2}^{2,g=2}$  ionization, reflecting a modest difference in proton affinity for the same Mn oxidation states in the different structures (Table S1). Thus, it appears that protonated and deprotonated W2 have similar energy in  $S_{2,g=2}^{2,g=2}$ . This is not well described by a W2  $pK_a$  near 6, as the protonation states of the highly coupled residues near the OEC do not titrate according to the Henderson–Hasselbalch equation. In the  $S_{2,g=4.1}^{2,g=4.1}$  state, with  $Mn4^{III}$ , the terminal waters are all neutral. Given the uncertainty of the protonation states of water, MCCE calculations were carried out with no constraints on the water protonation (free). In addition, for the



**Table 2** Protonation states of key residues near the OEC in the wild-type PSII

| S-state   | S <sub>1</sub>              | S <sub>1</sub>                                | S <sub>2</sub>                      | S <sub>2</sub>                      | S <sub>2</sub>                                | S <sub>2</sub>                                | S <sub>2</sub>                      | S <sub>2</sub>                                |
|---|-----------------------------|---|-------------------------------------|-------------------------------------|---|---|-------------------------------------|---|
| S <sub>structure</sub><br>redoxstate            | S <sub>1</sub> <sup>1</sup> | S <sub>1</sub> <sup>1</sup>                   | S <sub>2,g=2</sub> <sup>2,g=2</sup> | S <sub>2,g=2</sub> <sup>2,g=2</sup> | S <sub>2,g=2</sub> <sup>2,g=2</sup>           | S <sub>2,g=2</sub> <sup>2,g=2</sup>           | S <sub>2,g=2</sub> <sup>2,g=2</sup> | S <sub>2,g=4.1</sub> <sup>2,g=4.1</sup>       |
| Charge assignment                               | 3443                        | 3443  | 3444                                | 3444                                | 3444  | 3444  | 4443                                | 4443  |
| H190Y <sub>Z</sub>                              | Ground state                | H190 <sup>+</sup> Y <sub>Z</sub> <sup>·</sup> | Ground state                        | Ground state                        | H190 <sup>+</sup> Y <sub>Z</sub> <sup>·</sup> | H190 <sup>+</sup> Y <sub>Z</sub> <sup>·</sup> | Ground state                        | H190 <sup>+</sup> Y <sub>Z</sub> <sup>·</sup> |
| W2 constraint                                   | Free                        | Free  | Free                                | <i>H<sub>2</sub>O</i>               | Free  | <i>H<sub>2</sub>O</i>                         | Free                                | Free  |
| W1  | 0.00 ± 0.00                 | 0.00  | -0.08 ± 0.03                        | -0.26 ± 0.26                        | -0.52   | -0.16   | -0.01 ± 0.01                        | -0.01   |
| W2  | 0.00 ± 0.00                 | 0.00  | -0.80 ± 0.03                        | 0.00 ± 0.00                         | -0.48   | 0.00  | -0.01 ± 0.01                        | -0.08   |
| D1-D61  | -1.00 ± 0.00                | -1.00   | -0.92 ± 0.03                        | -0.74 ± 0.26                        | -0.48   | -0.84   | -0.99 ± 0.01                        | -0.99   |
| D1-H337   | 1.00 ± 0.00                 | 1.00  | 1.00 ± 0.00                         | 1.00 ± 0.00                         | 1.00  | 1.00  | 1.00 ± 0.00                         | 1.00  |
| D1-E329   | -0.71 ± 0.04                | -1.00   | -0.48 ± 0.06                        | -0.98 ± 0.17                        | -0.99   | -1.00   | -1.00 ± 0.00                        | -1.00   |
| D1-E65  | -1.00 ± 0.00                | -1.00   | -1.00 ± 0.00                        | -1.00 ± 0.00                        | -1.00   | -1.00   | -0.99 ± 0.005                       | -1.00   |
| D2-K317   | 1.00 ± 0.00                 | 1.00  | 1.00 ± 0.00                         | 1.00 ± 0.00                         | 1.00  | 1.00  | 1.00 ± 0.00                         | 1.00  |
| Charge (whole protein)                          | -33.54 ± 0.03               | -33.11  | -34.36 ± 0.08                       | -34.25 ± 0.12                       | -33.80  | -33.56  | -34.24 ± 0.04                       | -33.65  |
| Charge (residues near OEC)                      | -16.70 ± 0.04               | -17.00  | -17.28 ± 0.05                       | -16.99 ± 0.01                       | -17.47  | -17.00  | -17.00 ± 0.01                       | -17.08  |
| Change in H <sup>+</sup> (From S <sub>1</sub> ) |                             | -0.30   | -0.58                               | -0.28                               | -0.47   | -0.30   | -0.30                               | -0.38   |
| Sub-State                                       | 1                           | 2   | 3a                                  | 3b                                  | 4a  | 4b  | 3c                                  | 4c  |

H190Y<sub>Z</sub> ground states have both residues in their neutral form. W2 constraint: *Free* indicates that all groups are free to titrate, *H<sub>2</sub>O* W2 fixed as H<sub>2</sub>O (in italics)

Charge (whole protein) is the net charge of the full PSII. Charge (residues near OEC) considers OEC and a 15 Å region centered at the OEC from the D1, D2, and CP43 subunits listed in Methods section. Change in H<sup>+</sup> is the difference in total charge relative to that found in S<sub>1</sub><sup>1</sup> with neutral Y<sub>Z</sub> and H190. The standard deviation is for three independent MCCE calculations on the same structure. Values without a standard deviation represent a single calculation. H190<sup>+</sup>Y<sub>Z</sub><sup>·</sup>: Y<sub>Z</sub> is oxidized by P<sub>680</sub><sup>+</sup> before S-state advancement. The oxidized Y<sub>Z</sub> loses its proton to the nearby H190 forming H190<sup>+</sup>Y<sub>Z</sub><sup>·</sup>. State: There are multiple reaction paths through the table. For example, sub-states 1 → 2 → 3b → 3a → 4c move the system from S<sub>1</sub> to S<sub>1</sub>H190<sup>+</sup>Y<sub>Z</sub><sup>·</sup> to S<sub>2,g=2</sub> to S<sub>2,g=4.1</sub> to S<sub>2,g=4.1</sub>H190<sup>+</sup>Y<sub>Z</sub><sup>·</sup> with no proton loss from W2, while 1 → 2 → 3c → 3a → 4c allows proton loss from W2 in the S<sub>2,g=2</sub> state. The positive charge on Mn1 in S<sub>2,g=4.1</sub> or on H190<sup>+</sup>Y<sub>Z</sub><sup>·</sup> does not lead to proton release from W2 so no constraints on its protonation are applied to these calculations. Ionization in the intermediate region of a titration can be modified by small energy changes, while changes in ionization probability < 0.1 or > 0.9 reflect more consequential changes in free energy to significant digits are used to retain the latter information

S<sub>2,g=2</sub> state, W2 was fixed to be neutral to determine how this would influence the outcome.

MCCE results indicate that significantly less than 1 proton is lost during oxidation of S<sub>1</sub> to either form of the two S<sub>2</sub> redox isomers at pH 6, rather oxidation is accompanied by a redistribution of protons near the OEC. As the OEC goes from S<sub>1</sub><sup>1</sup> to S<sub>2,g=2</sub><sup>2,g=2</sup>, the average number of protons bound to the protein diminishes by 0.56 protons. W2 is hydroxyl in 80% of the Boltzmann distribution of microstates. In response, the probability of D1-E329 being protonated goes from 29% to 51%. There is also some proton transfer to D1-D61. While the exact probabilities vary with the initial structure, the relative importance of the residues involved in the transition do not (SI Table S1).

The calculations were also carried out with W2 constrained to be water. Here, comparing the number of protons bound in S<sub>1</sub><sup>1</sup> relative to S<sub>2,g=2</sub><sup>2,g=2</sup> or S<sub>2,g=4.1</sub><sup>2,g=4.1</sup> shows ≤ 0.3 protons are lost, in better agreement with experiment (Suzuki et al. 2009). Without the hydroxyl W2, the buildup of positive charge on the OEC causes D1-E329 to become fully deprotonated in the S<sub>2,g=2</sub> state and there is increased probability of proton transfer between W1 and D1-D61. Formation of

S<sub>2,g=4.1</sub><sup>2,g=4.1</sup> also leads to the release of 0.3 protons, almost entirely from D1-E329.

### Relative energy of S<sub>2,g=2</sub> and S<sub>2,g=4.1</sub> at pH 6

The measured redox potential for the S<sub>1</sub> → S<sub>i+1</sub> transition is determined by the free energy necessary to transform the structure and change protonation patterns as well as to oxidize the OEC. In the calculations discussed here this would represent the free energy change for the reaction S<sub>1</sub><sup>1</sup> → S<sub>2,g=2</sub><sup>2,g=2</sup> (SI Fig S1). However, MCCE is limited to calculations with a fixed OEC structure, restricting us to free energy calculations for oxidation of the reduced structure ( $E_{m,red}$  for S<sub>1</sub><sup>1</sup> → S<sub>2,g=2</sub><sup>2,g=2</sup>) and for the oxidized structure ( $E_{m,ox}$  for S<sub>1</sub><sup>2,g=2</sup> → S<sub>2,g=2</sub><sup>2,g=2</sup>) (Fig. 2, Table S3). The Linear Response Approximation, LRA, Fig. S1 (Makri 1999) uses the average of the  $E_m$  in the (fixed) reduced and (fixed) oxidized structures to provide an estimate of the  $E_m$  (denoted  $E_{m,LRA}$ ) (Russo et al. 2012; Zheng and Cui 2017). The MCCE calculated  $E_m$  values provide a relative electron affinity. An external benchmark value is required to fix the scale so that values can be reported relative to the standard hydrogen

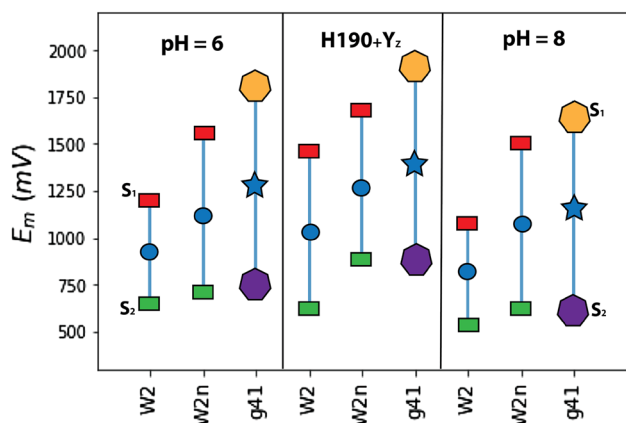


**Fig. 2** Relative  $E_m$  for oxidation of  $S_1$  to either of the  $S_2$  states. The  $E_{m,LRA}$  for  $S_1 \rightarrow S_{2,g=2}^1$  with W2 fixed as water (W2n) is taken as the reference state with an  $E_{m,LRA}$  of 1120 mV (Rappaport and Diner 2008). All calculations are at pH 6 unless noted. Red rectangle:  $E_{m,ox}$ :  $S_1^1 \rightarrow S_{2,g=2}^1$ ; Yellow heptagon:  $E_{m,ox}$ :  $S_1^1 \rightarrow S_{2,g=4.1}^1$ ; Green rectangle:  $E_{m,red}$ :  $S_1^{2,g=2} \rightarrow S_{2,g=2}^2$ ; Purple heptagon:  $E_{m,red}$ :  $S_1^{2,g=4.1} \rightarrow S_{2,g=4.1}^2$ ; Blue circle:  $E_{m,LRA}$  (average  $E_m$ ) for  $S_1 \rightarrow S_{2,g=2}$ ; Blue star:  $E_{m,LRA}$  (average  $E_m$ ) for  $S_1 \rightarrow S_{2,g=4.1}$ . Vertical line: range of  $E_m$  with  $S^1$  titration at the higher, more positive end and  $S^2$  titration at the lower end. W2:  $S_1 \rightarrow S_{2,g=2}$  with W2 is free; W2n:  $S_1 \rightarrow S_{2,g=2}$  with W2 fixed as  $H_2O$ ; g41:  $S_1 \rightarrow S_{2,g=4.1}$ . Free W2 remains neutral in  $S_1$  and  $S_{2,g=4.1}$  states. Additional perturbations:  $H190^+Y_Z$ ; calculations at pH 8. All values are given in SI Table S3

electrode. For ease of discussion, the  $E_{m,LRA}$  for  $S_1 \rightarrow S_{2,g=2}$  with W2 held neutral is fixed at the experimentally derived value of 1120 mV (Rappaport and Diner 2008).

The calculated redox potentials reflect that the lowest energy corresponds to the structure in which the system is optimized. Thus, the  $E_m$  to oxidize  $S_1$  to either of the  $S_2$  isomers is more positive in the  $S^1$  structure ( $E_{m,ox}$ ) and lower in either of the  $S^2$  structures ( $E_{m,red}$ ) (Fig. 2). The free energy difference between the two  $S_2$  isomers is given by the difference in their  $E_{m,LRA}$  (Fig. 2, Table S3). At pH 6, the  $E_{m,LRA}$  for  $S_1 \rightarrow S_{2,g=2}$  is lower than for  $S_1 \rightarrow S_{2,g=4.1}$  (Fig. 2), regardless of whether both waters on Mn4 are neutral or W2 partially ionized in  $S_{2,g=2}$ . Thus,  $S_{2,g=2}$  is thermodynamically more favorable than  $S_{2,g=4.1}$ . However, the free energy difference between  $S_{2,g=2}$  and  $S_{2,g=4.1}$  is larger when W2 becomes deprotonated than when W2 is fixed neutral (Fig. 2), as expected since the proton loss from the Mn4 primary ligand favors its oxidation.

The  $\Delta E_{m,LRA}$  between  $S_2$  isomers is compared to the  $\Delta E_m$  obtained from independent DFT-QM/MM calculations. The  $\Delta E_{m,LRA}$  obtained from the classical MCCE model within the protein is 158 mV while  $\Delta E_m$  between  $S_2$  isomers for the sphere obtained from QM/MM is 154 mV. Both calculations keep W2 neutral. The level of agreement certainly reflects some amount of error cancellation as the two calculation methods are quite different. For example, MCCE allows

for proton rearrangement on OEC oxidation, while the QM/MM has a more realistic model for the electron distribution over the cluster. However, the qualitative agreement shows convergence of simulations that place the  $S_{2,g=4.1}$  isomer at a similarly higher energy.

### Effect of oxidation of $Y_Z$

$Y_Z$  is oxidized and transfers a proton to D1-H190 to form  $H190^+Y_Z^{\bullet+}$  prior to each S-state transition. The proton loss on formation of  $H190^+Y_Z^{\bullet+}$  in the  $S_1$  state is equivalent to that found on forming either of the  $S_2$  states. Thus, with oxidation of  $Y_Z$  in the  $S_1$  state, D1-E329 is now fully deprotonated, as found in either of the  $S_2$  states (W2 fixed neutral). These changes found upon formation of  $H190^+Y_Z^{\bullet+}$  in the  $S_1$  state can help prepare the system for oxidation to  $S_{i+1}$  (Table 2), and are in agreement with experiments showing proton release precedes OEC oxidation (Dau et al. 2012; Zaharieva et al. 2016).

### pH dependence of $S_2$ isomer distribution

MCCE calculations compared PSII at pH 6 and pH 8 (Fig. 2). Overall, the protein has lost 20 protons as the pH is raised. However, the residues around the OEC do not lose protons, except for D1-E329 which is fully deprotonated at pH 8 in the  $S_1$  state (Table S4a). Thus, the local OEC environment is quite insensitive to changes of pH. The  $E_m$  for all states are  $\approx 50$ – $100$  mV lower at the higher pH. It is likely that the  $E_m$  for  $P_{680}$  and  $Y_Z$  will also be lowered leading to a smaller change in the overall reaction free energy. The  $\Delta E_{m,LRA}$  between the  $S_2$  isomers decreases, stabilizing formation of the  $S_{2,g=4.1}$  state, consistent with experiment (Boussac et al. 2018).

The change in proton loss going from  $S_1 \rightarrow S_2$  supports a role of D1-E329 as a buffer since it is predicted to be in a mixture of protonated and deprotonated states in  $S_1$  at pH 6 while fully deprotonated at pH 8 in either  $S_1$  or  $S_2$  states. When W2 is held neutral at pH 8, D1-E329 no longer has a proton to lose so now there is essentially zero proton loss moving from  $S_1$  to either of the  $S_2$  redox isomers. When W2 is free to deprotonate, the proton release to the lumen upon formation of the  $S_{2,g=2}$  state is more significant than at pH 6 since D1-E329 no longer binds a proton. Thus, the pH dependence of the reaction, especially at higher pH, can provide an experimental measure of the protonation state of W2 in  $S_2$ .

### Effect of chloride depletion

The protonation states of the nearby residues and the difference in energy between the  $S_{2,g=2}$  and  $S_{2,g=4.1}$  states were calculated with the two crystallographic  $Cl^-$  removed. The

removal of both chloride ions reduces the  $\Delta E_{m,LRA}$  between  $S_2$  isomers, which allows for the formation of more  $S_{2,g=4.1}$  (Fig. S2). This is observed when W2 is free or fixed neutral. In the absence of  $Cl^-$ , at least one proton is lost from the protein moving from  $S_1$  to either of the  $S_2$  states, suggesting this reaction will now be more pH dependent (Table S4a).  $Cl^-$  removal increases the ionization of D1-E329 in  $S_1$ , so this residue is no longer a buffer for protons. W2 is largely hydroxyl upon  $S_{2,g=2}$  formation. When W2 is fixed neutral, D2-K317 becomes fully deprotonated and there is additional proton transfer from W1 to D1-D61. In  $S_{2,g=4.1}$ , there is partial proton loss by D1-H337 as well as by W2 and some proton transfer from D2-K317 to D1-D61, indicating a stronger salt bridge between the Lys and Asp in either of the  $S_2$  states upon chloride depletion (Rivalta et al. 2011).

### Effect of mutagenesis studies on the $S_2$ isomers

#### D2-K317A

MCCE calculations were carried out in a D2-K317A mutant. As chloride is near D2-K317, multiple  $Cl^-$  positions were sampled and the optimal position shifts by  $\approx 0.5 \text{ \AA}$  (Fig. S3). The  $Cl^-$  binding affinity calculated in  $S_1^1$  is diminished by  $\approx 4 \text{ kcal/mol}$  in the mutant (Song and Gunner 2009; Chenal and Gunner 2017) in agreement with experiment that shows the  $Cl^-$  affinity is significantly diminished in this mutated PSII (Pokhrel et al. 2013).

With  $Cl^-$  present, the loss of the charge due to D2-K317A is calculated to be compensated for by an increase in the probability that D1-D61 and D1-E65 bind a proton (Table S4b). In  $S_{2,g=2}$  with W2 neutral, the redistribution of protons among these groups leads to loss of only 0.4 protons. When W2 is free in  $S_{2,g=2}$  or  $S_{2,g=4.1}$  there is more proton loss. Now with either  $S_{2,g=2}$  or  $S_{2,g=4.1}$  isomer, a fraction of W2, D1-E329, and D1-E65 become deprotonated, while D1-D61 becomes more protonated.

#### D1-D61A

D1-D61 is in a position to make a hydrogen bond to W1 and is close to D2-K317 and the primary  $Cl^-$  (Debus 2014). The most significant impact of removing D61 is that the proton affinity of both W1 and W2 is diminished. Upon formation of either of the  $S_2$  redox isomers, W1 or W2 loses, in aggregate, one proton that is not caught by other residues in the protein (Table S4b). This indicates the reaction will be more pH dependent in this mutant.

#### D1-S169A

D1-S169 is part of the narrow channel suggested to participate in water delivery (Askerka et al. 2015a). However, its

removal slightly raises the proton affinity of D1-E329 in the  $S_1$  state but not in either of the  $S_2$  states. The proton loss is relatively unchanged at 0.4 upon mutation (Table S4c).

### Equilibrium between $S_{2,g=2}$ and $S_{2,g=4.1}$ in mutants or $Cl^-$ depletion

Chloride depletion leads to an overall lowering of  $\Delta E_{m,LRA}$  between the  $S_{2,g=2}$  and  $S_{2,g=4.1}$  isomers, thereby favoring the  $S_{2,g=4.1}$  isomer (Table S4a). In addition, D1-D61A or D2-K317A changes the proton distribution in  $S_1$ , lowering the  $E_m$  for oxidation to either of the  $S_2$  states. Therefore, the  $\Delta E_{m,LRA}$  between the two redox isomers is little changed, continuing to favor  $S_{2,g=2}$  (Fig. S2). There is little difference in either the  $E_m$  or the  $\Delta E_m$ s upon D1-S169 mutation.

## Discussion

MCCE analysis has been carried out for the  $S_1$  and  $S_2$  states of PSII. This uses a Monte Carlo sampling with a classical force field. MCCE has the advantage of keeping the protonation states of the whole protein in equilibrium with the redox states of the OEC, allowing a more expansive look at the interaction between the protein and the OEC. While MCCE is routinely used to determine the protonation state of amino acids in proteins (Gunner et al. 2011; Nielsen et al. 2011), previous benchmark calculations on model oxo-Mn systems show the classical model is capable of estimating the proton affinity of terminal waters and the cluster  $E_m$  (Amin et al. 2013). The analysis of the water ligands on the OEC considers very large interactions between bonded atoms in the cluster so is it important to evaluate the sensitivity to small changes in structure. The proton distribution for each S-state with the geometry optimized in that S-state (Table 2) was compared with that obtained when the input structure was optimized in another state (SI Table S1). Fixing the oxidation state of the four Mn centers leads to essentially the same proton distribution, independent of the state in which the OEC has been subjected to QM/MM optimization. The variation between different structures is more likely to result from the random positions generated by MCCE conformational degrees of freedom that lead to small changes in the energies, which become important when the energy difference between protonated and deprotonated states is small. Likewise, the similar energy difference between the two redox isomers of  $S_2$  with W2 held as water calculated by QM/MM and MCCE lends support to the classical  $E_m$  calculations.

One of the open questions is the protonation states of terminal waters as the OEC cycles through different S-states. Standard QM/MM calculations have been used to calculate the relative energies (Ames et al. 2011) and to compare the

optimized structures to high-resolution EXAFS spectroscopy (Luber et al. 2011; Askerka et al. 2014, 2015a, b, 2016) in different protonation states. MCCE results indicate that the OEC charge distribution determines the water protonation states, independent of small changes in the underlying OEC structure. Thus, Monte Carlo sampling provides the Boltzmann distribution of water and hydroxyl for all 4 water ligands. They are all water in  $S_1$ , which is the protonation states of the input QM/MM calculations (Askerka et al. 2014, 2017). The  $Ca^{II}$  waters, W3 and W4, are always neutral in either of the  $S_2$  states as well. These results are consistent with experimental findings (Cox and Messinger 2013). When Mn1 is oxidized ( $S_{2,g=4.1}$ ) the waters bound to  $Mn4^{III}$ , W1 and W2, remain protonated. However, when Mn4 is oxidized ( $S_{2,g=2}$ ), a mixture of states is found with W2 having > 50% probability of being deprotonated. Thus, water or hydroxyl ligand to  $Mn4^{IV}$  are close in energy, while water is favored in the state with  $Mn4^{III}$ . Proton affinities of terminal waters in Mn model system can drop by more than 9 pH units on Mn oxidation (Limburg et al. 1999; Amin et al. 2013). If the two forms of W2 are this close in energy, it can help explain why different simulation techniques come to different conclusions about the W2 protonation state (Ames et al. 2011; Siegbahn 2013b; Bovi et al. 2013; Pokhrel and Brudvig 2014; Amin et al. 2015; Askerka et al. 2017).

The possibility of deprotonation of W2 in the  $S_{2,g=2}$  state has several ramifications. If W2 deprotonates when bound to  $Mn4^{IV}$  but not  $Mn4^{III}$ , then W2 is different in  $S_{2,g=2}$  and  $S_{2,g=4.1}$ . This is supported by several experiments. FTIR spectroscopy data find more asymmetric hydrogen bonding of waters in the  $S_{2,g=2}$  redox isomer (Noguchi and Sugiura 2000). In addition, the crystal structure of Ca-PSII (Umena et al. 2011) suggests that the distances of W1 and W2 from Mn4 are different, which is consistent with one water and one hydroxyl bound. In the crystal structure for Sr-PSII (Koua et al. 2013) the distances are more similar (Pokhrel and Brudvig 2014) consistent with both waters being neutral in the  $S_{2,g=4.1}$  redox isomer.

One of the unusual characteristics of the  $S_1 \rightarrow S_2$  transition is that little proton release (Suzuki et al. 2009) accompanies the oxidation of the OEC. This is in contrast to the other S-state transitions (Rappaport and Lavergne 1991; Lavergne and Junge 1993). MCCE finds that there is substoichiometric proton loss on formation of either of the  $S_2$  redox isomers. With 80% of W2 losing a proton, the probability of D1-E329 and D1-D61 being protonated increases so only 30% of the proteins will lose a proton to solution. If W2 remains neutral then D1-E329 is more like to be deprotonated again leading to a similar, modest proton loss. Thus, the surroundings buffer the system against losing a proton on forming  $S_2$  (Table 3).

At pH 6 in wild-type spinach little  $S_{2,g=4.1}$  is seen, while none is seen in cyanobacterial PSII (Pokhrel and Brudvig

**Table 3** Relative energies of the  $S_{2,g=2}$  and  $S_{2,g=4.1}$  redox isomers

|                                    | Expt                              | Free W2                     | W2 as $H_2O$         |
|------------------------------------|-----------------------------------|-----------------------------|----------------------|
| pH 6                               | Only $S_{2,g=2}$ <sup>a</sup>     | $S_{2,g=2}$                 | $S_{2,g=2}$          |
| Cl removed                         | Favors $S_{2,g=4.1}$ <sup>b</sup> | Favors $S_{2,g=4.1}$        | Favors $S_{2,g=4.1}$ |
| H190 <sup>+</sup> Y <sub>Z</sub> • | Only $S_{2,g=2}$ <sup>c</sup>     | Slightly favors $S_{2,g=2}$ | No change            |
| pH 8                               | Favors $S_{2,g=4.1}$ <sup>d</sup> | No change                   | Favors $S_{2,g=4.1}$ |
| D1-D61A                            | Only $S_{2,g=2}$ <sup>e</sup>     | No change                   | Favors $S_{2,g=2}$   |
| D2-K317A                           | Only $S_{2,g=2}$ <sup>f</sup>     | No change                   | Favors $S_{2,g=2}$   |
| D1-S169A                           | N.D                               | No change                   | No change            |

All simulations at pH 6 unless noted. Experimental measurements at pH 6 show only  $S_{2,g=2}$  indicating there is less than 10%  $S_{2,g=4.1}$  seen so the  $\Delta G$  is > 60 meV. Favors  $S_{2,g=4.1}$  indicate there is a mixture of both redox isomers seen. The calculated  $\Delta G$  between  $S_{2,g=2}$  and  $S_{2,g=4.1}$  is  $\approx 360$  meV with free W2 and  $\approx 160$  meV with W2 fixed as  $H_2O$ . No change indicates the free energy difference changes by < 10 meV; slightly favors: difference within 20 meV of the unperturbed calculation; favors  $S_{2,g=2}$  or favors  $S_{2,g=4.1}$  indicates a change > 20 meV. The  $\Delta\Delta G$  values can be found in S.I. Table S3<sup>a</sup>(Strickler et al. 2005),<sup>b</sup>(Ono et al. 1986),<sup>c</sup>(Dau and Haumann 2007),<sup>d</sup>(Boussac et al. 2018),<sup>e</sup>(Debus 2014),<sup>f</sup>(Pokhrel et al. 2013)

ND is not determined

2014; Vinyard et al. 2017; Boussac et al. 2018). It appears harder to generate the  $S_{2,g=4.1}$  signal in cyanobacteria than in spinach, indicating  $S_{2,g=2}$  may be more favored in the *Thermosynechococcus vulcanus* which is the source of the structure used here (Pokhrel and Brudvig 2014). The balance between the two redox isomers have been shown experimentally to be modulated by changes in solution conditions or by mutation (Pokhrel et al. 2013). At higher pH, the stable state is exclusively  $S_{2,g=4.1}$  in *Thermosynechococcus elongatus* cyanobacterial PSII (Boussac et al. 2018). As it has been suggested that  $S_3$  is formed via an initial, uphill transition to  $S_{2,g=4.1}$  (Pantazis et al. 2012; Cox and Messinger 2013; Bovi et al. 2013; Narzi et al. 2014; Vinyard et al. 2017; Boussac et al. 2018), tuning the balance of the two redox isomers would affect advancement rates along the S-state cycle.

The calculated  $\Delta G$  between  $S_{2,g=2}$  and  $S_{2,g=4.1}$  is  $\approx 360$  meV with free W2 (MCCE) and  $\approx 160$  meV with W2 fixed as  $H_2O$  (MCCE or QM/MM). Thus, deprotonation of W2 stabilizes  $S_{2,g=2}$ , and likely overestimates the  $\Delta G$ . In addition, with W2 fixed as water the  $\Delta G$  between the two redox isomers changes by  $\approx 30$ –120 meV as a function of mutation or pH, while with W2 free the  $\Delta G$  is more than 350 meV (Table S3), again highlighting the ability of proton to stabilize the oxidized state.

D2-K317, D1-D61, D1-S169, and Cl are close together near Mn4. D1-D61 can form hydrogen bond to W1 or to D2-K317. The proton distributions among these surrounding residues and W1 and W2 are highly interdependent and so are calculated to be modified by  $Cl^-$  removal or mutation of any individual residue.  $Cl^-$  depletions stabilized  $S_{2,g=4.1}$  relative to  $S_{2,g=2}$  but still blocks the



advancement beyond  $S_2$  (Ono et al. 1986; Yocum 2008). Previous calculations (Rivalta et al. 2011; Amin et al. 2016) have suggested that  $Cl^-$  blocks proton release via the narrow channel which may be required prior to oxidation to  $S_3$ . In contrast, mutation of D1-D61 (Debus 2014) or D2-K317 (Pokhrel et al. 2013) to Ala retains the  $S_{2,g=2}$  isomer even under conditions, such as  $Cl^-$  depletion, that enhance  $S_{2,g=4.1}$  formation in the wild-type PSII. Computational analysis (Rivalta et al. 2011) and subsequent experimental studies (Debus 2014) indicate that D1-D61 participates in the proton egress pathway so its mutation can decrease the efficiency of water oxidation. Thus, there is more than one way to slow the same reaction in this complex system. The binding affinity of chloride is also calculated to be diminished as a result of the Lys mutation, in agreement with the experimental results (Pokhrel et al. 2013). The calculations predict significantly more proton loss on advancing to  $S_2$  with either  $Cl^-$  depletion or D2-K317A mutation.

Prior to each S-state transition,  $Y_Z$  reduces  $P_{680}^+$  and transfers a proton to the adjacent D1-H190 forming the metastable  $H190^+Y_Z^\bullet$ . This process initiates changes that precede each S-state transition (Dau et al. 2012; Zahariva et al. 2016). MCCE sampling finds that  $Y_Z$  oxidation leads to additional proton release in either of the  $S_2$  redox isomers, in preparation for the next S-state (Table 2). However, the MCCE calculations see a small stabilization of the  $S_{2,g=2}$  isomer. A more stable  $S_{2,g=4.1}$  isomer, as found in ab-initio DFT calculations (Narzi et al. 2014), which do not allow proton rearrangement, would lower the barrier conversion to  $S_3$ , but is not required.

## Conclusions

Simulation can provide insight into the result of experiment. The classical MCCE analysis of the region around the OEC in wild-type and mutant PSII explores the relationship of shifting protonation states to the  $S_1$  to  $S_2$  transition. The Mn4 terminal ligand, W2, is neutral in  $S_1$  and  $S_{2,g=4.1}$ , while it is largely ionized in the  $S_{2,g=2}$  redox isomer and so its ionization state effects the favored  $S_2$  charge distribution. The partial ionization of W2 shows the water and hydroxyl forms are close in energy. D1-E329 plays a key role at pH 6, reducing the loss to solution in the formation of  $S_2$ , by catching protons lost from W2. The Glu D1-E329 is more likely to be deprotonated in the presence of  $H190^+Y_Z^\bullet$ , with proton release perhaps able to ease the transition to  $S_3$ . Analysis of the protonation states in PSII mutants and the effects of  $Cl^-$  removal shows the complex interactions among W1, W2,  $Cl^-$ , D1-D61, and D2-K317.

## Supporting Information (SI)

Additional information is provided in SI that includes the following: MCCE results with different input structures, Comparison of calculations in full PSII protein and QM/MM sphere at pH 6, Midpoint potential for oxidation of  $S_1$  to  $S_{2,g=2}$  or  $S_{2g=4.1}$ ,  $E_m$  for  $S_2/S_1$  for OEC in full PSII (mV), Determination of position of chloride ion for D2-K317A mutation, Protonation states of 15 Å sphere of residues from the D1, D2, and CP43 subunits with different perturbations, QM/MM methodology for free energy calculation.

**Acknowledgements** We would like to thank David Vinyard for very helpful discussion. We acknowledge financial support from the Division of Chemical Sciences, Geosciences, and Biosciences, Office of Basic Energy Sciences, U.S. Department of Energy, Photosynthetic Systems. Experimental work was funded by DE-FG02-05ER15646 (G. W. B.) and computational studies by DESC0001423 (M. R. G. and V. S. B.). M. R. G. also acknowledges infrastructure support from the National Institute on Minority Health and Health Disparities (Grant 8G12MD007603) from the National Institutes of Health. V. S. B. acknowledges DOE high-performance computing time from NERSC.

## Compliance with ethical standards

**Conflict of interest** The authors declare that they have no conflict of interest.

## References

- Ames W, Pantazis DA, Krewald V et al (2011) Theoretical evaluation of structural models of the  $S_2$  state in the oxygen evolving complex of photosystem II: protonation states and magnetic interactions. *J Am Chem Soc* 133:19743–19757. <https://doi.org/10.1021/ja2041805>
- Amin M, Vogt L, Vassiliev S et al (2013) Electrostatic effects on proton coupled electron transfer in oxomanganese complexes inspired by the oxygen-evolving complex of photosystem II. *J Phys Chem B* 117:6217–6226. <https://doi.org/10.1021/jp403321b>
- Amin M, Vogt L, Szejgis W et al (2015) Proton-coupled electron transfer during the S-state transitions of the oxygen-evolving complex of photosystem II. *J Phys Chem B* 119:7366–7377. <https://doi.org/10.1021/jp510948e>
- Amin M, Pokhrel R, Brudvig GW et al (2016) Effect of chloride depletion on the magnetic properties and the redox leveling of the oxygen-evolving complex in photosystem II. *J Phys Chem B* 120:4243–4248. <https://doi.org/10.1021/acs.jpcc.6b03545>
- Askerka M, Wang J, Brudvig GW, Batista VS (2014) Structural changes in the oxygen-evolving complex of photosystem II induced by the  $S_1$  to  $S_2$  transition: a combined XRD and QM/MM study. *Biochemistry* 53:6860–6862. <https://doi.org/10.1021/bi5011915>
- Askerka M, Vinyard DJ, Brudvig GW, Batista VS (2015a)  $NH_3$  binding to the  $S_2$  state of the  $O_2$ -evolving complex of photosystem II: analogue to  $H_2O$  binding during the  $S_2 \rightarrow S_3$  transition. *Biochemistry* 54:5783–5786. <https://doi.org/10.1021/acs.biochem.5b00974>
- Askerka M, Vinyard DJ, Wang J et al (2015b) Analysis of the radiation-damage-free X-ray structure of photosystem II in light of

- EXAFS and QM/MM data. *Biochemistry* 54:1713–1716. <https://doi.org/10.1021/acs.biochem.5b00089>
- Askerka M, Wang J, Vinyard DJ et al (2016) S<sub>3</sub> state of the O<sub>2</sub>-evolving complex of photosystem II: insights from QM/MM, EXAFS, and femtosecond X-ray diffraction. *Biochemistry* 55:981–984. <https://doi.org/10.1021/acs.biochem.6b00041>
- Askerka M, Brudvig GW, Batista VS (2017) The O<sub>2</sub>-evolving complex of photosystem II: recent insights from quantum mechanics/molecular mechanics (QM/MM), extended X-ray absorption fine structure (EXAFS), and femtosecond X-ray crystallography data. *Acc Chem Res* 50:41–48. <https://doi.org/10.1021/acs.accounts.6b00405>
- Baker NA, Sept D, Joseph S et al (2001) Electrostatics of nanosystems: application to microtubules and the ribosome. *Proc Natl Acad Sci USA* 98:10037–10041. <https://doi.org/10.1073/pnas.181342398>
- Becke AD (1988) Density-functional exchange-energy approximation with correct asymptotic behavior. *Phys Rev A* 38:3098–3100. <https://doi.org/10.1103/PhysRevA.38.3098>
- Boussac A, Ugur I, Marion A et al (2018) The low spin—high spin equilibrium in the S<sub>2</sub>-state of the water oxidizing enzyme. *Biochim Biophys Acta Bioenerg* 1859:342–356. <https://doi.org/10.1016/j.bbabi.2018.02.010>
- Bovi D, Narzi D, Guidoni L (2013) The S<sub>2</sub> state of the oxygen-evolving complex of photosystem II explored by QM/MM dynamics: spin surfaces and metastable states suggest a reaction path towards the S<sub>3</sub> state. *Angew Chem* 52:11744–11749. <https://doi.org/10.1002/anie.201306667>
- Casey JL, Sauer K (1984) EPR detection of a cryogenically photogenerated intermediate in photosynthetic oxygen evolution. *Biochim Biophys Acta* 767:21–28. [https://doi.org/10.1016/0005-2728\(84\)90075-6](https://doi.org/10.1016/0005-2728(84)90075-6)
- Chenal C, Gunner MR (2017) Two Cl ions and a glu compete for a helix cage in the CLC proton/Cl<sup>-</sup> antiporter. *Biophys J* 113:1025–1036. <https://doi.org/10.1016/j.bpj.2017.07.025>
- Cox N, Messinger J (2013) Reflections on substrate water and dioxygen formation. *Biochim Biophys Acta* 1827:1020–1030. <https://doi.org/10.1016/j.bbabi.2013.01.013>
- Cox N, Pantazis DA, Neese F, Lubitz W (2013) Biological water oxidation. *Acc Chem Res* 46:1588–1596. <https://doi.org/10.1021/ar3003249>
- Dau H, Haumann M (2007) Eight steps preceding O–O bond formation in oxygenic photosynthesis—a basic reaction cycle of the photosystem II manganese complex. *Biochim Biophys Acta* 1767:472–483. <https://doi.org/10.1016/j.bbabi.2007.02.022>
- Dau H, Zaharieva I, Haumann M (2012) Recent developments in research on water oxidation by photosystem II. *Curr Opin Chem Biol* 16:3–10. <https://doi.org/10.1016/j.cbpa.2012.02.011>
- Davis KM, Pushkar YN (2015) Structure of the oxygen evolving complex of photosystem II at room temperature. *J Phys Chem B* 119:3492–3498. <https://doi.org/10.1021/acs.jpcc.5b00452>
- De Paula JC, Brudvig GW (1985) Magnetic properties of manganese in the photosynthetic oxygen-evolving complex. *J Am Chem Soc* 107:2643–2648. <https://doi.org/10.1021/ja00295a016>
- Debus RJ (2014) Evidence from FTIR difference spectroscopy that D1-Asp61 influences the water reactions of the oxygen-evolving Mn<sub>4</sub>CaO<sub>5</sub> cluster of photosystem II. *Biochemistry* 53:2941–2955. <https://doi.org/10.1021/bi500309f>
- Debus RJ (2015) FTIR studies of metal ligands, networks of hydrogen bonds, and water molecules near the active site Mn<sub>4</sub>CaO<sub>5</sub> cluster in photosystem II. *Biochim Biophys Acta Bioenerg* 1847:19–34. <https://doi.org/10.1016/j.bbabi.2014.07.007>
- Dismukes GC, Siderer Y (1981) Intermediates of a polynuclear manganese center involved in photosynthetic oxidation of water. *Proc Natl Acad Sci USA* 78:274–278. <https://doi.org/10.1073/pnas.78.1.274>
- Gunner MR, Zhu X, Klein MC (2011) MCCE analysis of the pK<sub>s</sub> of introduced buried acids and bases in *Staphylococcal nuclease*. *Proteins* 79:3306–3319. <https://doi.org/10.1002/prot.23124>
- Joliet P (2005) Period-four oscillations of the flash-induced oxygen formation in photosynthesis. In: Govindjee, Beatty JT, Gest H, Allen JF (eds) *Discoveries in photosynthesis*. Springer, Berlin/Heidelberg, pp 371–378
- Jorgensen WL (1981) Quantum and statistical mechanical studies of liquids. 10. Transferable intermolecular potential functions for water, alcohols, and ethers. Application to liquid water. *J Am Chem Soc* 103:335–340. <https://doi.org/10.1021/ja00392a016>
- Kern J, Chatterjee R, Young ID et al (2018) Structures of the intermediates of Kok's photosynthetic water oxidation clock. *Nature* 563:421–425. <https://doi.org/10.1038/s41586-018-0681-2>
- Kok B, Forbush B, McGloin M (1970) Cooperation of charges in photosynthetic O<sub>2</sub> evolution-I. A linear four step mechanism. *Photochem Photobiol* 11:457–475
- Koua FHM, Umena Y, Kawakami K, Shen J-R (2013) Structure of Sr-substituted photosystem II at 2.1 Å resolution and its implications in the mechanism of water oxidation. *Proc Natl Acad Sci USA* 110:3889–3894. <https://doi.org/10.1073/pnas.1219922110>
- Krewald V, Retegan M, Cox N et al (2015) Metal oxidation states in biological water splitting. *Chem Sci* 6:1676–1695. <https://doi.org/10.1039/C4SC03720K>
- Lavergne J, Junge W (1993) Proton release during the redox cycle of the water oxidase. *Photosynth Res* 38:279–296. <https://doi.org/10.1007/BF00046752>
- Limburg J, Vrettos JS, Liable-Sands LM et al (1999) A functional model for O–O bond formation by the O<sub>2</sub>-evolving complex in photosystem II. *Science* 283:1524–1527. <https://doi.org/10.1126/science.283.5407.1524>
- Luber S, Rivalta I, Umena Y et al (2011) S<sub>1</sub>-state model of the O<sub>2</sub>-evolving complex of photosystem II. *Biochemistry* 50:6308–6311. <https://doi.org/10.1021/bi200681q>
- Makri N (1999) The linear response approximation and its lowest order corrections: An influence functional approach. *J Phys Chem B* 103:2823–2829. <https://doi.org/10.1021/jp9847540>
- Mao J, Hauser K, Gunner MR (2003) How cytochromes with different folds control heme redox potentials. *Biochemistry* 42:9829–9840. <https://doi.org/10.1021/bi027288k>
- Narzi D, Bovi D, Guidoni L (2014) Pathway for Mn-cluster oxidation by tyrosine-Z in the S<sub>2</sub> state of photosystem II. *Proc Natl Acad Sci USA* 111:8723–8728. <https://doi.org/10.1073/pnas.1401719111>
- Nielsen JE, Gunner MR, Bertrand García-Moreno E (2011) The pK<sub>a</sub> cooperative: a collaborative effort to advance structure-based calculations of pK<sub>a</sub> values and electrostatic effects in proteins. *Proteins* 79:3249–3259. <https://doi.org/10.1002/prot.23194>
- Noguchi T, Sugiura M (2000) Structure of an active water molecule in the water-oxidizing complex of photosystem II as studied by FTIR spectroscopy. *Biochemistry* 39:10943–10949. <https://doi.org/10.1021/bi001040i>
- Ono T, Zimmermann JL, Inoue Y, Rutherford AW (1986) EPR evidence for a modified S-state transition in chloride-depleted photosystem II. *Biochim Biophys Acta Bioenerg* 851:193–201. [https://doi.org/10.1016/0005-2728\(86\)90125-8](https://doi.org/10.1016/0005-2728(86)90125-8)
- Pantazis DA, Ames W, Cox N et al (2012) Two interconvertible structures that explain the spectroscopic properties of the oxygen-evolving complex of photosystem II in the S<sub>2</sub> state. *Angew Chem* 51:9935–9940. <https://doi.org/10.1002/anie.201204705>
- Pokhrel R, Brudvig GW (2014) Oxygen-evolving complex of photosystem II: correlating structure with spectroscopy. *Phys Chem Chem Phys* 16:11812–11821. <https://doi.org/10.1039/C4CP00493K>
- Pokhrel R, Service RJ, Debus RJ, Brudvig GW (2013) Mutation of lysine 317 in the D2 subunit of photosystem II alters chloride binding and proton transport. *Biochemistry* 52:4758–4773. <https://doi.org/10.1021/bi301700u>

- Rappaport F, Diner BA (2008) Primary photochemistry and energetics leading to the oxidation of the Mn<sub>4</sub>Ca cluster and to the evolution of molecular oxygen in photosystem II. *Coord Chem Rev* 252:259–272. <https://doi.org/10.1016/j.ccr.2007.07.016>
- Rappaport F, Lavergne J (1991) Proton release during successive oxidation steps of the photosynthetic water oxidation process: stoichiometries and pH dependence. *Biochemistry* 30:10004–10012. <https://doi.org/10.1021/bi00105a027>
- Renger G (2012) Mechanism of light induced water splitting in photosystem II of oxygen evolving photosynthetic organisms. *Biochim Biophys Acta Bioenerg* 1817:1164–1176. <https://doi.org/10.1016/j.bbabi.2012.02.005>
- Rivalta I, Amin M, Luber S et al (2011) Structural–functional role of chloride in photosystem II. *Biochemistry* 50:6312–6315. <https://doi.org/10.1021/bi200685w>
- Russo NVD, Estrin DA, Martí MA, Roitberg AE (2012) pH-dependent conformational changes in proteins and their effect on experimental pK<sub>a</sub>s: the case of nitrophorin 4. *PLoS Comput Biol* 8:e1002761. <https://doi.org/10.1371/journal.pcbi.1002761>
- Siegbahn PEM (2013a) Substrate water exchange for the oxygen evolving complex in PSII in the S<sub>1</sub>, S<sub>2</sub>, and S<sub>3</sub> states. *J Am Chem Soc* 135:9442–9449. <https://doi.org/10.1021/ja401517e>
- Siegbahn PEM (2013b) Water oxidation mechanism in photosystem II, including oxidations, proton release pathways, O–O bond formation and O<sub>2</sub> release. *Biochim Biophys Acta Bioenerg* 1827:1003–1019. <https://doi.org/10.1016/j.bbabi.2012.10.006>
- Song Y, Gunner MR (2009) Using multiconformation continuum electrostatics to compare chloride binding motifs in  $\alpha$ -amylase, human serum albumin, and omp32. *J Mol Biol* 387:840–856. <https://doi.org/10.1016/j.jmb.2009.01.038>
- Song Y, Mao J, Gunner MR (2009) MCCE2: improving protein pK<sub>a</sub> calculations with extensive side chain rotamer sampling. *J Comput Chem* 30:2231–2247. <https://doi.org/10.1002/jcc.21222>
- Strickler MA, Walker LM, Hillier W, Debus RJ (2005) Evidence from biosynthetically incorporated strontium and FTIR difference spectroscopy that the c-terminus of the D1 polypeptide of photosystem II does not ligate calcium. *Biochemistry* 44:8571–8577. <https://doi.org/10.1021/bi050653y>
- Suga M, Akita F, Hirata K et al (2015) Native structure of photosystem II at 1.95 Å resolution viewed by femtosecond X-ray pulses. *Nature* 517:99–103. <https://doi.org/10.1038/nature13991>
- Suzuki H, Sugiura M, Noguchi T (2009) Monitoring proton release during photosynthetic water oxidation in photosystem II by means of isotope-edited infrared spectroscopy. *J Am Chem Soc* 131:7849–7857. <https://doi.org/10.1021/ja901696m>
- Tannor DJ, Marten B, Murphy R et al (1994) Accurate first principles calculation of molecular charge distributions and solvation energies from ab initio quantum mechanics and continuum dielectric theory. *J Am Chem Soc* 116:11875–11882. <https://doi.org/10.1021/ja00105a030>
- Ullmann GM, Knapp E-W (1999) Electrostatic models for computing protonation and redox equilibria in proteins. *Eur Biophys J* 28:533–551. <https://doi.org/10.1007/s002490050236>
- Umena Y, Kawakami K, Shen J-R, Kamiya N (2011) Crystal structure of oxygen-evolving photosystem II at a resolution of 1.9 Å. *Nature* 473:55–60. <https://doi.org/10.1038/nature09913>
- Vinyard DJ, Brudvig GW (2017) Progress toward a molecular mechanism of water oxidation in photosystem II. *Annu Rev Phys Chem* 68:101–116. <https://doi.org/10.1146/annurev-physchem-052516-044820>
- Vinyard DJ, Khan S, Askerka M et al (2017) Energetics of the S<sub>2</sub> state spin isomers of the oxygen-evolving complex of photosystem II. *J Phys Chem B* 121:1020–1025. <https://doi.org/10.1021/acs.jpcc.7b00110>
- Wang L, Li L, Alexov E (2015) pK<sub>a</sub> predictions for proteins, RNAs, and DNAs with the Gaussian dielectric function using DelPhi pK<sub>a</sub>. *Proteins* 83:2186–2197. <https://doi.org/10.1002/prot.24935>
- Wang J, Askerka M, Brudvig GW, Batista VS (2017) Crystallographic data support the carousel mechanism of water supply to the oxygen-evolving complex of photosystem II. *ACS Energy Lett* 2:2299–2306. <https://doi.org/10.1021/acseenergylett.7b00750>
- Yano J, Yachandra V (2014) Mn<sub>4</sub>Ca cluster in photosynthesis: where and how water is oxidized to dioxygen. *Chem Rev* 114:4175–4205. <https://doi.org/10.1021/cr4004874>
- Yocum CF (2008) The calcium and chloride requirements of the O<sub>2</sub> evolving complex. *Coord Chem Rev* 252:296–305. <https://doi.org/10.1016/j.ccr.2007.08.010>
- Zaharieva I, Dau H, Haumann M (2016) Sequential and coupled proton and electron transfer events in the S<sub>2</sub> → S<sub>3</sub> transition of photosynthetic water oxidation revealed by time-resolved X-ray absorption spectroscopy. *Biochemistry* 55:6996–7004. <https://doi.org/10.1021/acs.biochem.6b01078>
- Zheng Y, Cui Q (2017) Microscopic mechanisms that govern the titration response and pK<sub>a</sub> values of buried residues in *Staphylococcal nuclease* mutants. *Proteins* 85:268–281. <https://doi.org/10.1002/prot.25213>
- Zhu Z, Gunner MR (2005) Energetics of quinone-dependent electron and proton transfers in *Rhodobacter sphaeroides* photosynthetic reaction centers. *Biochemistry* 44:82–96. <https://doi.org/10.1021/bi048348k>
- Zimmermann JL, Rutherford AW (1984) EPR studies of the oxygen-evolving enzyme of Photosystem II. *Biochim Biophys Acta Bioenerg* 767:160–167. [https://doi.org/10.1016/0005-2728\(84\)90091-4](https://doi.org/10.1016/0005-2728(84)90091-4)

**Publisher's Note** Springer Nature remains neutral with regard to jurisdictional claims in published maps and institutional affiliations.